ANNALS of the ORADEA UNIVERSITY.
Fascicle of Management and Technological Engineering

THIN GRANULAR LAYER ON A VIBRATING PLATE. GINZBURG-LANDAU EQUATION

Mircea Bogdan TATARU
University of Oradea, btataru@uoradea.ro

Key words: stripes, squares, hexagons, interfaces, oscillons, superoscillons

Abstract: A theoretical study of patterns in vibrated granular layers is presented. An order parameter model based on the parametric Ginzburg-Landau equation is used to describe strongly nonlinear excitations including stripes, squares, hexagons, interfaces between flat anti-phase domains, and new localized objects, oscillons and superoscillons.

1. Introduction

Poligranular material separation using vibrating separating surfaces, like plates with holes or reticular membranes (sieve tissues) employs knowing behaviour and dynamics of granular material in this processing devices. The collective dynamics of granular materials is a subject of current interest [1–6]. The intrinsic dissipative nature of the interactions between the constituent macroscopic particles gives rise to several basic properties specific to granular substances which set granular matter apart from conventional gaseous, liquid, or solid states. Driven granular systems manifest collective fluid-like behavior: convection, surface waves, and pattern formation (see e.g., reference [1, 2]). One of the most fascinating examples of collective dynamics in these materials is the appearance of long-range coherent patterns and localized excitations in vertically vibrated thin granular layers [3–9]. In this paper we describe high-acceleration patterns on the basis of the same order parameter model and compare it with experimental observations. Preliminary results were published earlier in references [6, 16, 17]. Here we show that at large amplitude of driving both hexagons and interfaces emerge. It was found a morphological instability leading to the formation of ‘‘decorated’’ interfaces. It was studied the motion of the interface under the influence of a small subharmonic component in the driving acceleration. It was also found a new localized structure, a ‘‘superoscillon,’’ which exists for high acceleration values. They discussed possible mechanisms of saturation of the interface instability. The experimental results demonstrate the existence of superoscillons and bound states of superoscillons and interfaces. They also confirm theoretical predictions for the external control of interface motion.

2. Parametric Ginzburg - Landau equation

Pattern formation in thin layers of granular material were studied theoretically by several groups. The equations of motion following from the symmetry arguments and mass conservation reproduced the essential phenomenology of patterns near the threshold of the primary bifurcation: stripes, squares, and, localized objects, oscillons.

The essence of the model [15, 16] is the first order parameter equation for the complex amplitude y of parametric layer oscillations $h = y\,.\exp(ipft) + \text{c.c.}$ at the frequency $f/2$ coupled with the equation for the thickness of the layer r averaged over the period of vibrations:

$$\partial_t y = g.y^* - (1 - iw).y + (1 + ib).\nabla^2 y - |y|^2 y - r\,y \qquad (1)$$

$$\partial_t r = a\nabla.\left(r\nabla|y|^2\right) + b.\nabla^2 r \tag{2}$$

Here g is the normalized amplitude at is forcing at the frequency, f. Linear terms in equation (1) can be obtained from the complex growth rate for infinitesimal periodic layer perturbations, $h \sim \exp[\Lambda(k).t + ikx]$. Expanding $\Lambda(k)$ for small k, and keeping only two leading terms in the expansion $\Lambda(k) = -\Lambda_o - \Lambda_1 k^2$ we obtain the linear terms in equation (1), where $b = \operatorname{Im}\Lambda_1 / \operatorname{Re}\Lambda_1$ characterizes the ratio of dispersion to diffusion and parameter $w = (\Omega_o - p.f)/\operatorname{Re}\Lambda_o$, $\Omega_o = -\operatorname{Im}\Lambda_o$ characterizes the frequency of the driving. In equation (2), z and b are transport coefficients for, r. The slowly varying thickness of the layer r controls the dissipation rate (the last term in equation (1)). The second equation (2) describes the redistribution of the averaged thickness due to the diffusive flux $\propto -\nabla r$, and an additional flux $\propto -r\nabla|y|^2$ caused by the spatially non-uniform vibrations of the granular material. This coupled model was used in references [15, 16] to describe pattern selection near the threshold of the primary bifurcation. It was shown that at small $z.r_o b^{-1}$ (which corresponds to low frequencies and thick layers) the primary bifurcation is subcritical, and leads to the emergence of square patterns. For higher frequencies and/or thinner layers, the transition is supercritical and leads to roll patterns. At intermediate frequencies ($f \approx f^*$), the stable localized solutions of equations (1) and (2), corresponding to isolated oscillons and a variety of bound states, were found to be in agreement with experiment.

In this paper, we focus on high acceleration patterns at high frequencies. In reference [15] it was indicated that the density transport coefficient b is proportional to the energy of the plate vibration, $(\propto A^2 f^2)$, where A is the amplitude of the vibration, therefore, it should increase with the driving frequency f. As a result, for high frequencies the coupling between r and y becomes less relevant, and one can assume $r = \text{const.}$ and exclude it from equation (1) by rescaling. Then the model may be reduced to a single order parameter equation:

$$\partial_t y = g.y^* - (1 - iw).y + (1 + ib).\nabla^2 y - |y|^2 y \tag{3}$$

Equation (3) also describes the evolution of the order parameter for the parametric instability in vertically oscillating fluid layers (see references [18, 19]).

It is convenient to shift the phase of the complex order parameter via $\tilde{y} = y.\exp(if)$ with $\sin 2f = w/g$. The equations for the real and imaginary parts of $\tilde{y} = A + iB$ are:

$$\partial_t A = (s-1).A - 2w.B - \left(A^2 + B^2\right).A + \nabla^2(A - b.B) \tag{4}$$

$$\partial_t B = -(s+1).B - \left(A^2 + B^2\right).B + \nabla^2(B + b.A) \tag{5}$$

where $s^2 = g^2 - w^2$.

3. Uniform states stability

At $s < 1$, equations (4) and (5) have only one trivial uniform state $A = 0, B = 0$. At, $s > 1$, two new uniform states appear: $A = \pm\sqrt{s-1}$, $B = 0$. The onset of these states corresponds to the period doubling of the layer flights sequence, as observed in experiments [3], and predicted by the simple inelastic ball model [3, 20]. Signs $\pm$ reflect two relative phases of layer flights with respect to container vibrations [21].

The trivial flat state $A = B = 0$ loses stability if the following condition is fulfilled (compare with reference [15]):

$$g^2 > \frac{(w+b)^2}{1+b^2} \tag{6}$$

Because of the symmetry of equation (3), small perturbations from the trivial state lead to the formation of a periodic sequence of rolls or stripes.

Let us analyze the stability of the nontrivial states $A = \pm\sqrt{s-1}$ and $B = 0$ with respect to small perturbations with wave number, k:

$$\begin{pmatrix} A \\ B \end{pmatrix} = \begin{pmatrix} \pm\sqrt{s-1} \\ 0 \end{pmatrix} + \begin{pmatrix} U_k \\ V_k \end{pmatrix} \exp\left[l(k).t + ikx\right] \tag{7}$$

The uniform state loses its stability with respect to periodic modulations with the critical wave number k_C at $s < s_C$ (correspondingly, $g < g_C$), where:

$$s_C = \frac{\sqrt{(1+w^2)(1+b^2)} - w + b}{2b} \tag{8}$$

$$k_C^2 = -\frac{2s - 1 - w.b}{1+b^2} \tag{9}$$

Small perturbations in every direction of the wave vector grow at the same rate. Nonlinear competition between the modes determines the resultant selected pattern. In the presence of the reflection symmetry, $y \to -y$, quadratic nonlinearity is absent and cubic nonlinearity near the trivial state favors stripes corresponding to a single mode. Near the fixed points $A = \pm\sqrt{s-1}$, $B = 0$ the reflection symmetry for perturbations $U \to -U$, $V \to -V$ is broken, and hexagons emerge at the threshold of the instability.

To clarify this point we perform a weakly nonlinear analysis of equations (4) and (5) for $s = s_C - e$ and $e << 1$. At $e \to 0$, the variables U and V are related as in a linear system:

$$\begin{pmatrix} U \\ V \end{pmatrix} = \begin{pmatrix} 1 \\ h \end{pmatrix} \Psi$$

$$\Psi = \sum A_j \exp\left[i.\mathrm{k}.\mathrm{r}\right] + \mathrm{c.c.} \tag{10}$$

where $|k| = k_C$ and $h = \left[2.(s_C - 1) + k_C^2\right] / \left(b.k_C^2 - 2.w\right)$.

The corresponding adjoint eigenvector is:

$$\begin{pmatrix} U^+ \\ V^+ \end{pmatrix} = \begin{pmatrix} 1 \\ h^+ \end{pmatrix} \tag{11}$$

where $h = -\left[2.(s_C - 1) + k_C^2\right]/b.k_C^2$. Substituting equation (10) into equations (4) and (5) and performing the orthogonalization, we obtain equations for the slowly varying complex amplitudes A_j, $j = 1, 2, \text{and } 3$ (we assume only three waves with triangular symmetry, favored by quadratic nonlinearity):

$$\partial_t A_j = 2e.A_j + a_2 A_{j+1}^* A_{j-1}^* - a_3\left[\left|A_j\right|^2 + 2\left(\left|A_{j-1}\right|^2 + \left|A_{j+1}\right|^2\right)\right] A_j \tag{12}$$

where a_2 and a_3 are the coefficients:

$$a_2 = \pm 2.\sqrt{s-1} \cdot \left(2 + \frac{1+h^2}{1+hh^+}\right), \quad a_3 = 3.\left(1 + hh^+\right) \tag{13}$$

Equations (12) were well studied (see reference [22]). There exist three critical values of e: $e_A = -a_2^2/40a_3$, $e_R = a_2^2/2a_3$, $e_B = 2a_2^2/a_3$. Hexagons are stable for, $e_A < e < e_B$, and stripes are stable for $e > e_R$. Thus, near $s = s_C$ the model exhibits stable hexagons [23]. Since we have two symmetric fixed points, both "up" and "down" hexagons coexist. For smaller s stripes are stable, and for larger s flat layers are stable, in agreement with observations [4, 17] as well as direct numerical simulations of equation (3) [24]. The above analysis requires the values of $e_{A,B,R}$ to be small. For parameters, $w, b = O(1)$, this requirement is satisfied for e_A, but not for $e_{B,R}$. The estimates may be improved by substituting $s = s_C + \in$ instead of $s = s_C$ in equation (13). The resulting range of stable hexagons is plotted in the phase diagram (w, g) (see Fig. 7 below).

4. Interface solution

At $s > 1$, equations (4) and (5) have an interface solution connecting two uniform states $A = \pm\sqrt{s-1}$, $B = 0$. Let x be the coordinate perpendicular to the interface and y the parallel coordinate. The interface is the stationary solution to equations (4) and (5):

$$\begin{aligned} &(s-1).A_0 - 2wB_0 - \left(A_0^2 + B_0^2\right).A_0 + A_{0xx} - bB_{0xx} = 0, \\ &-(s+1).B_0 - \left(A_0^2 + B_0^2\right)B_0 + B_{0xx} + bA_{0xx} = 0. \end{aligned} \tag{14}$$

For, $b = 0$, equations (14) have a solution of the form: $A_0 = \pm\sqrt{s-1}.th\left(\sqrt{s-1}.x/2\right)$, $B_0 = 0$. For, $b \neq 0$ the solution is available only numerically. Was used the shooting matching technique to find this solution in the range of parameters, w, b, and g. A typical solution is shown in Fig. 1. As one sees from the figure, for $b \neq 0$ the asymptotic behavior of the interface exhibits decaying oscillations.

Let us now consider the perturbed solution:

$$\begin{pmatrix} A \\ B \end{pmatrix} = \begin{pmatrix} A_0 \\ B_0 \end{pmatrix} + \begin{pmatrix} \tilde{A}(x) \\ \tilde{B}(x) \end{pmatrix} \exp\left[l(k).t + iky\right] \tag{15}$$

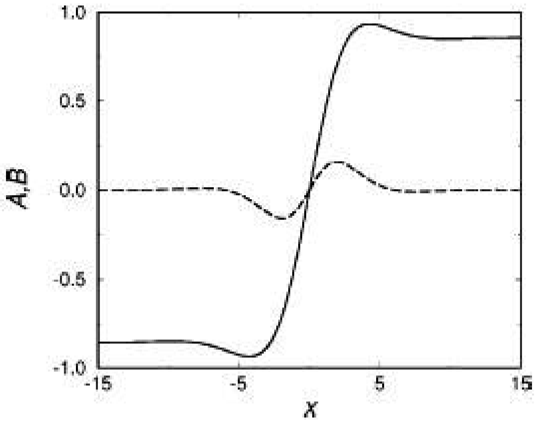

Fig. 1. Interface solution to equations (14) obtained numerically for, $w = 1$, $b = 4$***, and*** $g = 2$***. The solid line corresponds to*** A ***and the dashed line to*** B***, respectively.***

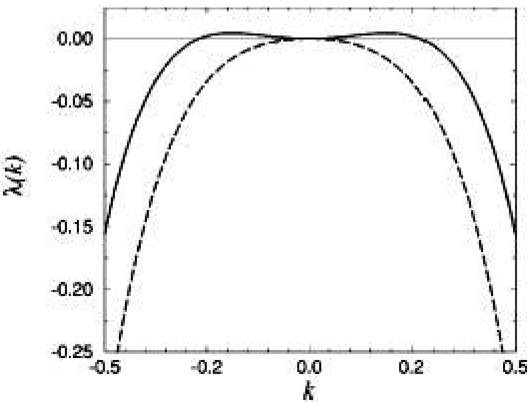

Fig. 2., Spectrum of eigenvalues $l(k)$ ***for*** $w = 1{,}3$, $b = 4$***, and*** $g = 2$ ***(solid line) and*** $w = 1$, $b = 4$***, and*** $g = 2$ ***(dashed line) obtained from numerical solution of equation (16).***

where, k is the transverse modulation wave number and, $l(k)$ is the corresponding growth rate. For $\tilde{A}$ and $\tilde{B}$ we obtain the linear equation:

$$\hat{L}\begin{pmatrix} \tilde{A} \\ \tilde{B} \end{pmatrix} = \left[l(k) + k^2\right] \cdot \begin{pmatrix} \tilde{A} \\ \tilde{B} \end{pmatrix} + bk^2 \begin{pmatrix} \tilde{B} \\ -\tilde{A} \end{pmatrix} \tag{16}$$

where, $\hat{L}$ is the matrix of the form:

$$\hat{L} = \begin{pmatrix} s - 1 - 3A_0^2 - B_0^2 + \partial_x^2 & -2w - 2A_0 B_0 - b\partial_x^2 \\ -2A_0 B_0 + b\partial_x^2 & -s - 1 - A_0^2 - 3B_0^2 + \partial_x^2 \end{pmatrix} \tag{17}$$

In order to determine the spectrum of eigenvalues, $l(k)$ we have solved equation (16) along with stationary equations (14) numerically using numerical matching-shooting technique. We have found that for small w the interface is stable with respect to transverse undulations, i.e., $l(k) \le 0$. However, for the values of w above certain critical value $w_C(g, b)$ the interface exhibits transverse instability: $l(k) > 0$ in the band of wave numbers $|k| < k_C$; see Fig. 2.

This instability is confirmed by direct numerical simulations of equation (3). An example of the evolution of slightly perturbed interface is shown in Fig. 4. Small perturbations grow to form a ‘‘decorated’’ interface. With time these decorations evolve slowly, and eventually form a labyrinthine pattern.

The neutral curve for this instability can be determined as follows. Numerical analysis shows that at the threshold the most unstable wave number is $k = 0$, and we can expect that, for $k \to 0$, $?\sim k^2$; see Fig. 2. Expanding equation (16) in a power series of k^2, in the zero order in, k

$$\begin{pmatrix} \tilde{A} \\ \tilde{B} \end{pmatrix} = \begin{pmatrix} A^{(0)} \\ B^{(0)} \end{pmatrix} + k^2 \begin{pmatrix} A^{(0)} \\ B^{(0)} \end{pmatrix} + \ldots, \tag{18}$$

we obtain $\hat{L}\left(A^{(0)}, B^{(0)}\right) = 0$. The corresponding solution is the translation mode, $A^{(0)} = \partial_x A_0(x)$, $B^{(0)} = \partial_x B_0(x)$. In the first order in k^2 we arrive at the linear inhomogeneous problem:

$$\hat{L}\begin{pmatrix} A^{(1)} \\ B^{(1)} \end{pmatrix} = \left[l(k) + k^2\right] \cdot \begin{pmatrix} A^{(0)} \\ B^{(0)} \end{pmatrix} + bk^2 \begin{pmatrix} B^{(0)} \\ -A^{(0)} \end{pmatrix} \tag{19}$$

A bounded solution to equation (19) exists if the right hand side is orthogonal to the localized mode of the ad-joint operator $A^\dagger$, $B^\dagger$. The ad-joint operator $\hat{L}^\dagger$ is of the form:

$$\hat{L}^\dagger = \begin{pmatrix} s - 1 - 3A_0^2 - B_0^2 + \partial_x^2 & -2A_0 B_0 + b\partial_x^2 \\ -2w - 2A_0 B_0 - b\partial_x^2 & -s - 1 - A_0^2 - 3B_0^2 + \partial_x^2 \end{pmatrix} \tag{20}$$

Since the operator $\hat{L}^\dagger$ is not self ad-joint, the ad-joint mode does not coincide with the translation mode, and, therefore, must be obtained numerically.

The orthogonality condition fixes the relation between l and k:

$$l = -s.k^2, \quad s = 1 + b\frac{\int_{-\infty}^{\infty}\left[A^{(0)}.B^\dagger - B^{(0)}.A^\dagger\right]dx}{\int_{-\infty}^{\infty}\left[A^{(0)}.A^\dagger + B^{(0)}.A^\dagger\right]dx} \tag{21}$$

where s is ‘‘surface tension’’ of the interface. The instability, corresponding to the negative surface tension of the interface, onsets at $s = 0$. Although the interface solution $A(x)$ is not localized (see Fig. 1), the integrals in equation (21) converge because the ad-joint functions $A^\dagger$ and $B^\dagger$ are localized. The numerically obtained ad-joint eigenmode is shown in Fig. 3. The neutral curve is shown in Fig. 7. Direct numerical simulations of equation (3) show that this instability leads to so called ‘‘decorated’’ interfaces (see Fig. 4(a)); however, at later stages the undulations grow and finally form labyrinthine patterns (Figs. 4(b)–4(d)).

The emergence of the labyrinthine patterns as a result of interface instability contradicts experiments [5, 6, 17] where stable decorated interfaces are typically observed. Thus the model, equation (3), does not capture saturation of the interface instability and requires modification. We also checked that the coupling to the density field introduced in reference [15] does not provide desired saturation.

Let us now discuss possible mechanisms of saturation of the transverse instability of the interface, which is not captured by equation (3). The reason for the proliferation of the “labyrinths” is that local stabilization mechanisms cannot saturate the ‘‘negative surface tension instability’’ of the interface. Indeed, the behavior of the small perturbation z of an almost flat interface is described by the linear equation, $z_t = -s.\Delta z$, where s is the surface tension. The linear growth must counterbalance nonlinear terms. Due to translation invariance the local nonlinearity can be a function of gradients of z only. In the lowest order the first term is, $|\nabla z|^3$, since the quadratic term does not saturate the monotonic instability.

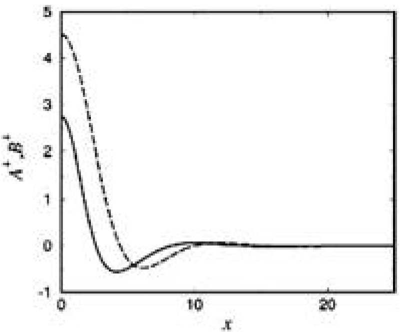

Fig. 3. Ad-joint eigenfunction obtained numerically for $w = 1{,}3$, $b = 4$, and $g = 2$. The solid line corresponds to $A^\dagger$ and the dashed line to $B^\dagger$, respectively

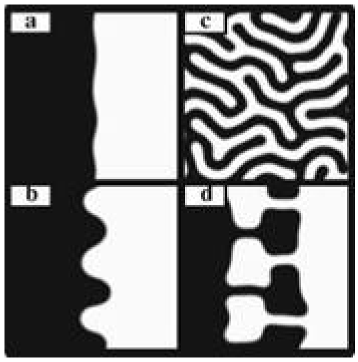

Fig. 4. (a)–(d) Interface instability and labyrinth formation, equation (3), $w = 2$, $b = 4$, and $g = 2{,}9$, the domain size is 100×100 units, and snapshots are taken at times $t = 1000, 1600, 2300$ and 4640

Since for the modulation wave number, $k \to 0$ one has $|\nabla z|^3 \sim k^2 |z|^3$ and $\Delta z \sim k^2 z$, the linear instability always overcomes the local nonlinearity at small wave numbers. As a result, small perturbations grow and saturation occurs due to non-local interactions as in a labyrinthine pattern which is stabilized by non-local repulsion of the fronts (see reference [22]).

As we see in our model, the interface instability does not result in stable decorated interfaces. One possibility for the saturation of this instability could be local convection induced by the interface. Indeed, due to the shear motion of grains at the interface (the flat regions move in anti-phase) local convective flow can be created. The scale of this flow can be larger than the interface thickness. One of the possible manifestations of the convection beside grain transport is a reduction of the effective ‘‘viscosity’’ of the flat layer, or an increase in the sensitivity to external vibrations [23]. As we can see from Fig. 7, an increase in vibration magnitude g suppresses the interface instability. As the instability develops, the length of the interface grows which increases the convection and finally suppresses the instability. This feedback mechanism results in a saturation of the interface instability, and creates stable decorations.

Although the details of this coupling are not yet known, it can be implemented within the first order parameter approach in a phenomenological way. In equation (3) the forcing gy^* must be replaced by, $(g_0 + w)y^*$, where w includes the effect of local convective flow and, $g_0 = \text{const}$. We take the simplest possible form of the coupling to the convective flow:

$$w = \frac{e}{S}\int dr'.exp\left(-\frac{|r-r'|^2}{r_0^2}\right)|\nabla y(r')|^2, \tag{22}$$

where r_0 characterizes the typical scale of the convective flow, e is the amplitude of the coupling, and S is the area of integration domain. Since $|\nabla y(r')|$ is non-zero only at the interface, this integral is proportional to the total length of the interface. With the growth of the interface length the value of the ‘‘effective forcing’’ $g = g_0 + w$ grows as well, and eventually leaves the instability domain.

We performed numerical simulations with equation (3) modified in the following way. The convolution integral (22) was calculated using the fast Fourier transform (FFT). The results are presented in Fig. 5. Remarkably, for a certain range of parameters the instability indeed saturates due to the non-local term equation (22), and we find interfaces with stable decorations; see Fig. 5(a).

5. Localized solutions

In addition to the interface solution which exists for $s > 1$, for even higher values of s equation (3) possesses a variety of other nontrivial two dimensional solutions including localized superoscillons. A typical solution and its corresponding localized linear mode are shown in Fig. 6.

Although superoscillons appears to be similar to the ‘‘conventional oscillon” discovered in reference [5], there is a significant difference. The asymptotic behavior of the superoscillon is $\Psi \to A_0 \neq 0$ for $r \to \infty$, whereas the regular oscillon has $\Psi \to 0$.

This implies that the phase of the superoscillon is always locked into the phase of the flat layer exhibiting *period-doubled behavior*, whereas “conventional oscillons’’ of either phase coexist on the harmonic background (the amplitude of period of 2 oscillations is zero). As a result oppositely phased superoscillons must be separated by an interface connecting two opposite phases of the period-doubled flat layer, whereas oppositely phased oscillons can easily form stable bound states (dipoles [5]).

Superoscillons, in the presence of additional subharmonic driving, are somewhat similar to normal oscillons of like polarity (see reference [5]). In this case the external driving creates a period-doubled background of the flat layer, and locks the phase of the superoscillons. However, superoscillons exist for parameter values where the oscillons of reference [5] are impossible even with additional subharmonic driving.

Superoscillons exist in a relatively narrow domain of parameters of equations (3). A decrease of g leads to a destabilization of the localized eigenmode leading to a subsequent nucleation of new ‘‘superoscillons’’ on the periphery of the unstable superoscillon; with an increase of g superoscillons disappear in a saddle-node bifurcation.

For certain values of g_0 we also find an interesting structure consisting of *a* decorated interface and a chain of superoscillons bound to the decorations; see Fig. 5(b). These objects can exist completely independently of the interface Fig. 5(c), as one may expect for equation (3). Thus we conclude that the extended equation (3) qualitatively describes the observed phenomenology.

6. Phase diagram

The results of a linear stability analysis can be summarized in the phase diagram shown in Fig. 7. Remarkably, the structure of the phase diagram of Fig. 7 is qualitatively similar to that of experiments for high frequencies of vibration; see references [3–6, 11, 17]. Increasing the vibration amplitude g leads to a transition from a trivial state to stripes, hexagons, decorated interfaces, and, finally, to stable interfaces. A transition from unstable to stable interfaces also occurs with decreasing w (increasing vibration frequency, f), in agreement with references [17, 23]. In experiments at still higher Γ’s, quarter harmonic patterns appear; however, these patterns are not described by our model. This analysis also predicts the coexistence of stripes and hexagons in a very narrow parameter range (see section 3). Superoscillons were found in a narrow domain close to line 7 of Fig. 7.

Note that square patterns, which emerge at lower frequencies, are not included in the phase diagram. They are obtained within the full model of equations (1) and (2), with an additional density field, r ; see references [15].

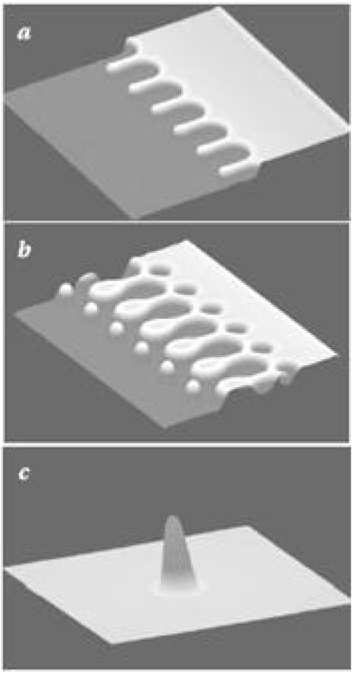

Fig. 5. Computer simulations of modified equation (3). Surface plots show $\mathrm{Re}\,\Psi$ ***for different stationary solutions: (a) A saturated interface;*** $w = 1{,}2$, $g = 1{,}85$, $b = 4$, $\in = 0{,}002$, $r_0 = 40$, ***and*** $L = 160$. ***(b) A saturated interface with bound superoscillons;*** $w = 1{,}2$, $g = 1{,}75$, $b = 4$, $\in = 0{,}002$, $r_0 = 40$, ***and*** $L = 160$. ***(c) A single superoscillon at*** $w = 1{,}2$, $g = 2{,}2$, $b = 4$, $\in = 0{,}002$, $r_0 = 40$, ***and*** $L = 100$.

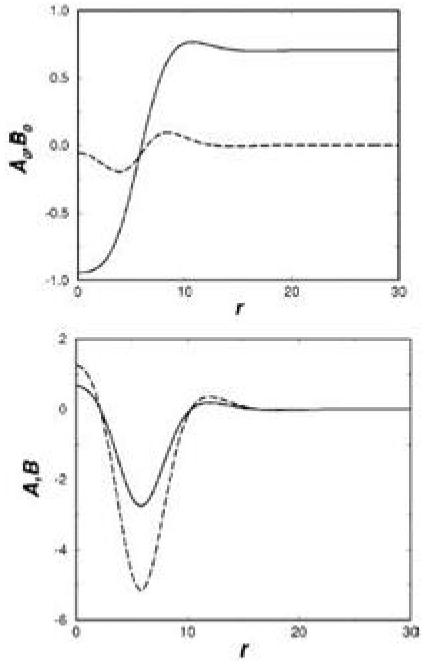

Fig. 6. (a) Axisymmetric localized solution (superoscillon) obtained for, $b = 4$, $w = 2$, ***and*** $g = 2{,}9$ ***for equation (3) at*** $b = 4$. ***A, solid line; B, dashed line. (b) Localized eigen-function corresponding to the maximum eigen-value*** $l = -0{,}0009$.

7. Conclusions

In this paper we studied the dynamics of thin vibrated granular layers in the framework of a phenomenological model based on the Ginzburg-Landau-type equation for an order parameter characterizing the amplitude of subharmonic sand vibrations. Although a rigorous derivation of this model is not possible to date, our approach gives a significant insight into the problem at hand, and results in testable predictions. Our model is complementary to more elaborate fluid dynamic-like continuum descriptions (or direct molecular dynamics simulations), and allows us to carry out analytical calculations of various regimes and predict their stability. A challenging problem is to establish a quantitative relation between our order-parameter model and other models as well as experiments.

We have shown in this paper that the *generic parametric Ginzburg-Landau model* of equation (3) captures not only patterns of vibrated sand near the primary bifurcation, but also large acceleration patterns such as hexagons, interfaces, and superoscillons. The

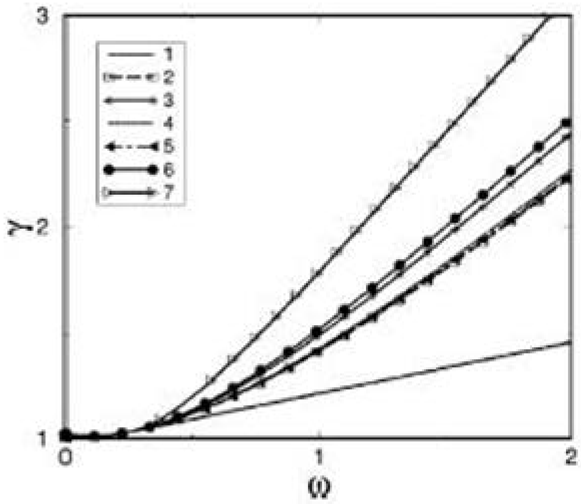

Fig. 7. - Phase diagram for equation (3) at $b=4$: Line 1, $g^2=(w+b)^2/(1+b^2)$; line 2, $s^2=g^2-w^2=1$; line 3, $s=s_C$; line 4, $s=s_C-\in_R$; line 5, $s=s_C-\in_B$; line 6, $s=s_C-\in_A$; line 7, surface tension $s=0$. Below line 1 there are no patterns. Between lines 1 and 4, stripes are stable. Between lines 5 and 6, hexagons are stable. Above line 2, nontrivial flat states exist. Above line 3 these states are stable. Interfaces are unstable below line 7. Hexagons and stripes coexist between lines 4 and 5.

structure of the phase diagram of Fig. 7 for high frequencies and amplitudes of vibrations is qualitatively similar to that of previous experiments (references [2], [3], [5], [16]).

Increasing the vibration amplitude leads to a transition from a trivial state to stripes, hexagons, decorated interfaces, and finally, to stable interfaces. Interface decorations were found to be a result of the transversal instability of a flat interface, which is analogous to the negative surface tension. We found that equation (3) is not sufficient to describe the saturation of the interface instability.

References

1. Blair, D, Aranson, I. S., G. W. Crabtree, Vinokur, V., Tsimring, L. S.,. Josserand, C, Patterns in thin vibrated granular layers: Interfaces, hexagons, and superoscillons, *Phys. Rev. E*, 61, 5600 **(2000).**
2. Jaeger, H.M., Nagel, S.R., Behringer, R.P.,Phys. Today 49 (4), 32 (1996); Rev. Mod. Phys. 68, 1259 (**1996).**
3. Melo, F., Umbanhowar, P.B., Swinney, H.L., Phys. Rev. Lett. 72, 172 **(1994).**
4. Melo, F., Umbanhowar, P.B., Swinney, H.L., Phys. Rev. Lett. 75, 3838 **(1995).**
5. Umbanhowar, P.B., Melo, F., Swinney, H.L., Nature (London) 382, 793 **(1996)**; Physica A 249, 1 **(1998).**
6. Aranson, I.S., Blair, D., Kwok, W., Karapetrov, G., Welp, U., Crabtree, G.W., Vinokur, V.M., Tsimring, L.S., Phys. Rev. Lett. 82, 731 **(1999).**
7. Metcalf, T.H., Knight, J.B., Jaeger, H.M., Physica A 236, 202 **(1997).**
8. Mujica N., Melo, F., Phys. Rev. Lett. 80, 5121 **(1998).**
9. Wassgren, C.R., Brennen, C.E., Hunt, M.L., J. Appl. Mech. 63, 712 **(1996)).**
10. Bizon, C., Shattuck, M.D., Swift, J.B., McCormick, W.D., Swinney, H.L., Phys. Rev. Lett. 80, 57 **(1998).**
11. De Bruyn, J.R., Bizon, C., Shattuck, M.D., Goldman, D., Swift, J.B., Swinney, H.L., Phys. Rev. Lett. 81, 1421 **(1998**).
12. Luding, S., Clement, E., Rajchenbach, J., Duran, J., Europhys. Lett. 36, 247 **(1996).**
13. Rothman, D.,Phys. Rev. E 57, 1239 **(1998)**; E. Cerda, F. Melo, and S. Rica, Phys. Rev. Lett. 79, 4570 **(1997)**; Shinbrot, T., Nature (London) 389, 574 (1997); J. Eggers and H. Riecke, Phys. Rev. E 59, 4476 **(1999)**; S. C. Venkataramani and E. Ott, Phys. Rev. Lett. 80, 3495 **(1998).**
14. Crawford C.,and H. Riecke, Physica D 129, 83 **(1999).**
15. Tsimring L.S., and I.S. Aranson, Phys. Rev. Lett. 79, 213 **(1997)**; I.S. Aranson and L.S. Tsimring, Physica A 249, 103 **(1998)**.
16. Aranson, I.S., L.S. Tsimring, and V.M. Vinokur, Phys. Rev. E 59, 1327 **(1999)**.
17. Das, P.K.and D. Blair, Phys. Lett. A 242, 326 **(1998)**.
18. Zhang W., and J. Vinals, Phys. Rev. Lett. 74, 690 **(1995).**
19. Kiyashko, S.V., L.N. Korzinov, M.I. Rabinovich, and L.S. Tsimring, Phys. Rev. E 54, 5037 **(1996).**
20. Mehta A., and J.M. Luck, Phys. Rev. Lett. 65, 393 **(1990)**.
21. Cross M., and P.C. Hohenberg, Rev. Mod. Phys. 65, 851 **(1993)**.
22. Petrich D.M., and R.E. Goldstein, Phys. Rev. Lett. 72, 1120 **(1994)**; R.E. Goldstein, D.J. Muraki, D.M. Petrich, and Phys. Rev. E 53, 3933 **(1996)**.
23. Umbanhowar, P.B., Ph. thesis, University of Texas, Austin, **(1996)**.

***) Papers are referenced in apparition order**